BIOCHEMISTRY
including biophysical chemistry & molecular biology

Article

pubs.acs.org/biochemistry

Structural Features of LC8-Induced Self-Association of Swallow

Ariam I. Kidane,[†] Yujuan Song,[†] Afua Nyarko,[†] Justin Hall,[†,§] Michael Hare,[†] Frank Löhr,[‡] and Elisar Barbar*,[†]

[†]Department of Biochemistry and Biophysics, Oregon State University, Corvallis, Oregon 97331, United States
[‡]Institute of Biophysical Chemistry, Goethe-University, D-60438 Frankfurt, Germany

ABSTRACT: Cell functions depend on the collective activity of protein networks within which a few proteins, called hubs, participate in a large number of interactions. Dynein light chain LC8, first discovered as a subunit of the motor protein dynein, is considered to have a role broader than that of dynein, and its participation in diverse systems fits the description of a hub. Among its partners is Swallow with which LC8 is essential for proper localization of *bicoid* mRNA at the anterior cortex of *Drosophila* oocytes. Why LC8 is essential in this process is not clear, but emerging evidence suggests that LC8 functions by promoting self-association and/or structural organization of its diverse binding partners. This work addresses the energetics and structural features of LC8-induced Swallow self-association distant from LC8 binding. Mutational design based on a hypothetical helical wheel, intermonomer nuclear Overhauser effects assigned to residues expected at interface positions, and circular dichroism spectral characteristics indicate that the LC8-promoted dimer of Swallow is a coiled coil. Secondary chemical shifts and ^{15}N backbone relaxation identify the boundaries and distinguishing structural features of the coiled coil. Thermodynamic analysis of Swallow polypeptides designed to decouple self-association from LC8 binding reveals that the higher binding affinity of the engineered bivalent Swallow is of purely entropic origin and that the linker separating the coiled coil from the LC8 binding site remains disordered. We speculate that the LC8-promoted coiled coil is critical for *bicoid* mRNA localization because it favors structural organization of Swallow, which except for the central LC8-promoted coiled coil is primarily disordered.

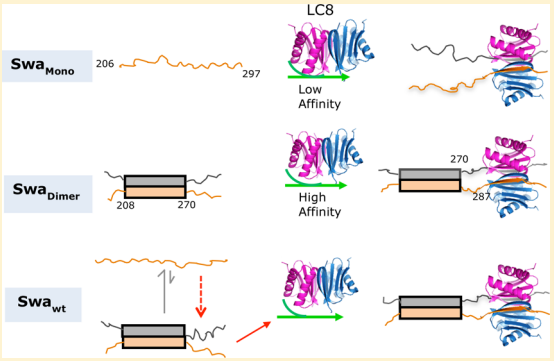

Swallow is a 62 kDa multidomain protein with a predicted α-helical coiled coil centered between primarily disordered N- and C-terminal domains (Figure 1). Synthesized by maternal nurse cells in the egg chamber, Swallow is exported to the interconnected oocyte compartment during *Drosophila* oogenesis,[1−3] where it is required for proper localization of several mRNAs such as *bicoid* mRNA (*bcd* mRNA), *huli-tai shao*-adducin-like mRNA (*htsN4* mRNA), and Oskar.[4,5] The localization of *bcd* mRNA in the anterior cortex of the *Drosophila* oocytes establishes a morphogenetic gradient of bicoid protein, which determines the anterior−posterior embryonic pattern.[6,7] In Swallow mutants with deletions in the predicted coiled-coil domain or truncations in the C-terminal domain, *bcd* mRNA fails to localize but spreads uniformly throughout the oocyte cytoplasm, resulting in embryonic anterior defects.[1] Additionally, Swallow mutants affect mislocalization of *htsN4* mRNA, causing cytoskeleton anomalies and consequent nuclear cleavage and migration defects.[4]

Swallow sequence analysis revealed a recognition sequence for dynein light chain LC8 at the C-terminal end of the predicted coiled coil.[1] LC8 (DYNLL1 in mammals) is a highly conserved 10.3 kDa homodimeric protein that assembles in the molecular motor dynein by binding intermediate chain IC.[8−10] LC8 was first described in dynein and was widely viewed as a dynein cargo adaptor.[11] Binding of Swallow to LC8 fostered the hypothesis that *bcd* mRNA cargo is transported by dynein through its interaction with Swallow.[1,3] However, crystal structures of LC8 bound to Swallow and IC peptides later showed that both partners bind the same symmetrical grooves at the LC8 dimer interface.[8,12,13] Moreover, LC8 in both cases binds two chains of the same protein and promotes their self-association distant from the LC8−Swallow interface,[9,14] arguing against the one-groove, one-peptide model;[15] therefore, LC8 cannot simultaneously bind to dynein and to Swallow, implying both dynein and dynein-independent LC8 functions.[8,16] Consistent with dynein-independent LC8−Swallow association, recent reports indicate that Swallow and *bcd* mRNA are transported independently and *bcd* mRNA along with the protein Staufen are carried by dynein to the anterior pole, where Swallow is already localized.[17] Instead of directly binding to *bcd* mRNA and dynein, Swallow appears to be involved in the stabilization of microtubules associated with the transport of *bcd* mRNA.[4,17,18]

What exactly is the role of LC8 in the LC8−Swallow interaction? Insight into this question is given from an analysis of LC8 and more than 20 LC8−partner proteins involved in essential and diverse cellular processes,[16] including chromo-

Received: May 22, 2013
Revised: August 3, 2013
Published: August 5, 2013

   dx.doi.org/10.1021/bi400642u | *Biochemistry* 2013, 52, 6011−6020

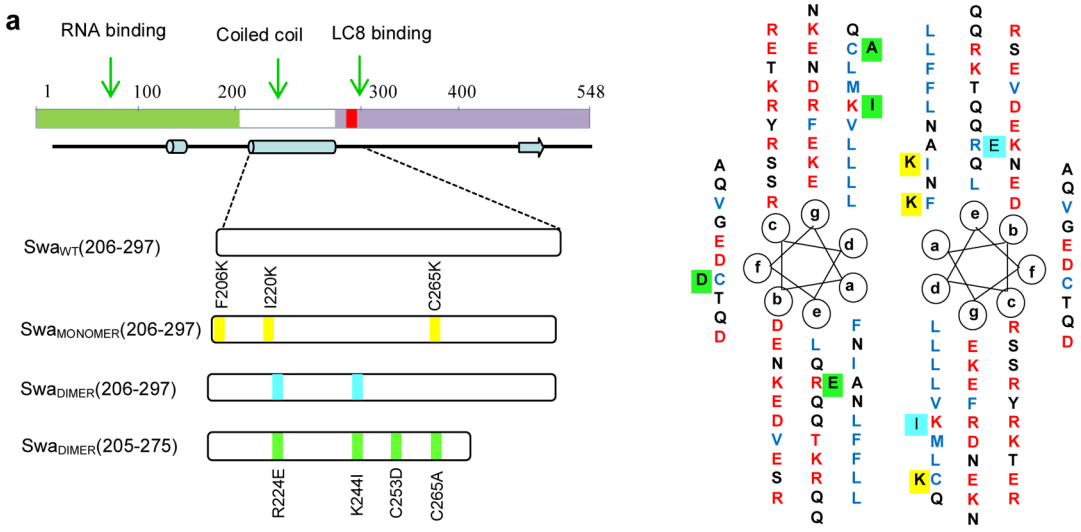

Figure 1. Schematic representation of full-length *Drosophila* Swallow protein and constructs used in this work. (a) Full-length *Drosophila* Swallow includes a putative RNA-binding domain at the N-terminus (green), a predicted α-helical coiled-coil region (residues 205−275) (white), and an LC8 recognition sequence (red) with the canonical KATQT motif (residues 291−295). Predicted secondary structural elements[42] are shown as a cylinder for helix, an arrow for strand, and a solid line for disorder. Site-specific mutations that promote monomer (yellow) or dimer (turquoise and green) formation are indicated on the schematic of the constructs used in this work. (b) Hypothetical helical wheel representation of the predicted coiled-coil region. Positions in the heptad repeats are denoted by a−g. Charged, hydrophobic, and neutral residues are colored red, blue, and black, respectively. Positions of the monomer- and dimer-promoting mutations are highlighted, yellow and turquoise in one chain and green in the second chain.

some segregation, mitotic spindle assembly,[19] and apoptosis,[20] where deletion or overexpression of LC8 causes cell apoptosis or breast cancer cell malignancy.[20,21] These diverse interactions led to the hypothesis that LC8 functions as a regulatory hub protein in a number of essential systems by facilitating the assembly and stabilization of its primarily disordered partners.[16] Such a role was clearly demonstrated for the interaction of LC8 with dynein IC and with nuclear pore complex subunit Nup159: in both instances, LC8 binding promotes self-association and higher-order assembly of its partners.[22−24] In the case of Swallow, biophysical characterization of its predicted coiled-coil domain shows that this domain is primarily monomeric at room temperature and that LC8 binding is required for its self-association and stability (the melting temperatures with and without LC8 are 15 and 45 °C, respectively).[14]

Here we expand our studies of the LC8−Swallow interface[8,12] and the observation that LC8 promotes Swallow self-association[14] to identification of the structural features of the self-association domain promoted by LC8 and the energetics of its formation. We demonstrate by mutational design and intermonomer NOEs that the self-association domain is a coiled coil as predicted and identify by secondary chemical shifts and backbone dynamics the boundaries and distinguishing structural features of this domain. Thermodynamic analysis of Swallow constructs designed to decouple self-association from LC8 binding reveals that LC8 binding enhances self-association by an entropic bivalency effect and gives a measure of the extent of self-association. Because residues predicted to form a coiled-coil domain are essential for the proper functioning of Swallow,[1] our working model is one in which LC8 binding promotes the formation of the coiled coil, which in turn is necessary for the regulation of long-range events associated with structural organization of the disordered N- and C-terminal domains.

MATERIALS AND METHODS

Construct Design and Protein Preparation. The regions corresponding to Swallow residues 205−275 and 206−297 were amplified by polymerase chain reaction and subcloned into Champion pET-SUMO (Invitrogen) and pET 15 (Novagen) vectors, respectively. Multi-site-directed mutagenesis was performed to generate Swa$_{DIMER}$(206−297), Swa$_{MONOMER}$(206−297), and Swa$_{DIMER}$(205−275) with two (R224E/K244I), three (F206K/I220K/C265K), and four (R224E/K244I/C253D/C265A) mutations, respectively. Two coexpressed constructs were also generated by subcloning LC8 or its phosphomimetic mutant (S88E)[25] with Swa$_{WT}$ (amino acids 206−297) into a pETDuet-1 coexpression vector (Novagen). The sequences of all constructs were verified prior to transformation into *Escherichia coli* BL21(DE3) for protein expression.

Cells were grown at 37 °C in LB for Swa$_{WT}$, Swa$_{DIMER}$(206−297), Swa$_{MONOMER}$(206−297), pETDuet-1 Swa$_{WT}$/LC8, and Swa$_{WT}$/LC8-S88E or in MJ9 medium containing $^{15}NH_4Cl$ and [^{12}C]- or [^{13}C]glucose for Swa$_{DIMER}$(205−275) to an OD$_{600}$ of 0.6−0.8. Protein expression was induced by 0.2 mM isopropyl β-D-galactopyranoside, and cells were grown for an additional 4 h at 37 °C for Swa$_{MONOMER}$(206−297) or 16 h at 18 °C for Swa$_{DIMER}$(206−297), Swa$_{DIMER}$(205−275), Swa$_{WT}$/LC8, and Swa$_{WT}$/LC8-S88E. Cells were harvested, resuspended in lysis buffer [50 mM sodium phosphate (pH 8.0), 500 mM NaCl, 10 mM imidazole, 5 mM β-mercaptoethanol, and a protease inhibitor cocktail], disrupted by sonication, and centrifuged, and the protein was purified using Ni-NTA affinity resin (Qiagen). Swa$_{MONOMER}$(206−297) expressed in inclusion bodies was purified under denaturing conditions. The SUMO tag of Swa$_{DIMER}$(205−275) was removed following Invitrogen's protocols. After the final purification on a Superdex 75 (16/60) column (GE Healthcare), the proteins were dialyzed in appropriate buffers and their purity and molecular weights were confirmed by matrix-assisted laser desorption ionization

dx.doi.org/10.1021/bi400642u | *Biochemistry* 2013, 52, 6011−6020

time-of-flight mass spectrometry. Protein concentrations were determined from the absorbance at 280 nm.

Size Exclusion Chromatography and Multiangle Laser Light Scattering (MALLS). The association states of $Swa_{DIMER}(206-297)$ and $Swa_{MONOMER}(206-297)$ mutants were determined from analytical size exclusion chromatography on a Superdex 75 HR analytical column (GE healthcare) with an online multiangle laser light scattering detector (miniDawn, Wyatt Technology). The running buffer consisted of 200 mM sodium sulfate, 50 mM sodium phosphate, 1 mM sodium azide (pH 7.3), and 5 mM β-mercaptoethanol; 100 or 200 μL of protein samples was injected at a flow rate of 0.5 mL/min at room temperature at a loading protein concentration in the range of 100−500 μM. Samples were monitored by UV absorption at 220 or 280 nm and by the refractive index. For $Swa_{DIMER}(205-275)$, several buffer conditions were tested to identify 20 mM MES with 10 mM NaCl (pH 5.6) as the appropriate buffer that gives a homogeneous dimer with no higher-order aggregates at concentrations suitable for NMR studies. The MALLS-determined molecular mass of $Swa_{DIMER}(205-275)$ is 20 kDa, consistent with the theoretical value of 18 kDa expected for a dimer. Data were processed using ASTRA version 5.1.9.1 (Wyatt Technology).

Circular Dichroism. CD spectra were recorded on a Jasco720 spectropolarimeter using a water bath and water-jacketed cells for temperature control. Samples were prepared in 10 mM sodium phosphate buffer with 30 mM NaCl (pH 7.8) in the protein concentration range of 3−30 μM. Thermal unfolding was measured by monitoring the CD signal at 222 nm in the temperature range of 5−83 °C, allowing equilibration for 3 min per 3 °C temperature increment. Reversibility was determined by comparing measurements taken at 5 °C before and after thermal unfolding. The fraction of folded $Swa_{MONOMER}(206-297)$ was determined from comparison to the CD signal of $Swa_{DIMER}(206-297)$ at similar concentrations.

Isothermal Titration Calorimetry. Proteins were dialyzed in PBS containing an additional 5% (v/v) glycerol, 5 mM β-mercaptoethanol, and 1 mM benzamidine (pH 7.4). Thermodynamics of binding were determined at 20, 25, 30, and 35 °C using a VP-ITC isothermal titration calorimeter from MicroCal (Northampton, MA) and processed using Origin version 7.0 (OriginLab Corp., Northampton, MA). Data were fit to a single-site binding model (A + B → AB, where A and B refer to a single chain of Swallow and LC8, respectively). The heat of dilution, estimated to be less than the enthalpy of the final injection, was subtracted from the data prior to fitting.

All ITC experiments were conducted with Swallow proteins in the sample cell and LC8 in the syringe using cell and syringe concentrations of 0.003 and 0.1, 0.03 and 0.5, and 0.02 and 0.5 mM for Swa_{WT}/LC8, $Swa_{MONOMER}(206-297)$/LC8, and $Swa_{DIMER}(206-297)$/LC8, respectively. The "c value" ($c = [\text{protein}]_{\text{sample cell}} K_d^{-1}$) was between 3 and 30, 30 and 85, and 17 and 420 for Swa_{WT}, $Swa_{MONOMER}(206-297)$, and $Swa_{DIMER}(206-297)$, respectively. The c values for the interactions with Swa_{WT} are the lowest because of its limited solubility. Changes in heat capacity at constant pressure (ΔC_p) were determined from the slope of the change in enthalpy ($\Delta H°$) as a function of temperature. All ΔC_p values were obtained with linear correlation coefficients of ≥0.93.

NMR Experiments and Analysis. Doubly ^{15}N- and ^{13}C-labeled samples of $Swa_{DIMER}(205-275)$ were prepared at a protein concentration of 0.5 mM in MES buffer [20 mM MES, 10 mM NaCl, and 1 mM sodium azide (pH 5.6)], protease inhibitors, and 4,4-dimethyl-4-silapentane-1-sulfonic acid (DSS) for referencing of ^1H chemical shifts. $^1H-^{15}N$ HSQC spectra were recorded at 10, 20, 30, and 40 °C, with the spectrum at 40 °C showing the best resolution and largest number of peaks. Therefore, all subsequent experiments were conducted at 40 °C.

A series of BEST−TROSY NMR experiments,[26] including HNCACB, HN(CO)CACB, TROSY-H(CCCO)NH-TOCSY, (H)CC(CO)NH-TOCSY, and HAHB(CBCACO)NH, were conducted to determine the backbone assignments on Bruker spectrometers in the field range of 600−950 MHz. NMR spectra were processed with TopSpin (Bruker) and analyzed with Sparky[27] or NMRView.[28]

Secondary structure propensities for $Swa_{DIMER}(205-275)$ were determined from SSP using the Cα and Cβ chemical shifts.[29] Negative scores correspond to β-strands, while positive scores correspond to α-helices.[29] Coiled-coil prediction of $Swa_{DIMER}(205-275)$ was performed using Coils.[30]

NMR dynamics data were derived from the measurement of ^{15}N relaxation, including R_1, R_2, and steady-state heteronuclear NOE on a Varian 800 MHz instrument. R_1 and R_2 relaxation values were recorded at 40 °C at time points of 0, 100, 200, 400, 600, 800, 1100, 1500, and 1900 ms for R_1 and 30, 50, 70, 90, 100, 130, 170, 210, and 250 ms for R_2. R_1 and R_2 values were determined by fitting peak heights versus time profiles to the formula $I = I_0 \times \exp(-tR)$ using the rate analysis interface in NMRView,[28] where I_0 is the initial peak intensity and I is the intensity measured at time t. Curve fitting and standard deviations were calculated with NMRView.[28] NOE values were obtained from the ratios of peak intensities in the presence and absence of amide proton saturation. Standard deviations were determined from the intensities of the baseline noise using the formula $\sigma/\text{NOE} = [(\sigma I_{sat}/I_{sat})^2 + (\sigma I_{unsat}/I_{unsat})^2]^{1/2}$, where I and σI correspond to the intensity of the peak and its baseline noise, respectively.

A three-dimensional (3D) $\omega 1$-$^{13}C/^{15}N$-filtered, ^{13}C-separated NOESY-HSQC spectrum[31] was recorded at 900 MHz on a $Swa_{DIMER}(205-275)$ sample prepared by mixing equimolar amounts of ^{13}C- and ^{15}N-labeled and unlabeled protein in 4 M urea, 50 mM phosphate, and 150 mM NaCl (pH 8.0). The dimeric protein was then reconstituted by dialysis in 20 mM MES and 10 mM NaCl (pH 8.0) and concentrated to 0.8 mM.

RESULTS

Design of Swallow Constructs That Promote or Disrupt Coiled-Coil Stability. The construct Swa(206−297) (termed Swa_{WT}) includes the predicted coiled coil (residues 206−275) and the LC8 recognition sequence (residues 287−296).[8,14] The construct $Swa_{DIMER}(206-297)$ includes two mutations that promote coiled-coil stability: R224 [position e on a hypothetical helical wheel (Figure 1b)] was replaced with Glu (turquoise) to minimize charge−charge repulsion upon interaction with K219 at position g of the opposite chain, and K244 (position d) was replaced with Ile (turquoise) to remove a charged residue from the putative hydrophobic interface upon formation of a coiled coil. The construct $Swa_{MONOMER}(206-297)$ includes three mutations that disrupt formation of a coiled coil: F206 and I220 (both at positions a) and C265 (position d) were all replaced with Lys (yellow) that inhibits formation of a coiled coil to avoid charge−charge repulsion at the interface. To facilitate structural studies at concentrations suitable for NMR, a shorter construct that contains only the predicted coiled-coil domain

dx.doi.org/10.1021/bi400642u | Biochemistry 2013, 52, 6011−6020

Swa_{DIMER}(205−275) was made. Swa_{DIMER}(205−275) is a model of the LC8-bound Swallow as it includes the R224E and K244I dimer stabilizing mutations. Additionally, it includes the C253D and C265A (green) mutations that prevent aggregation caused by disulfide bond formation at NMR concentrations.

Association State(s), Structure, and Stability. Association states of Swallow mutants were determined from size exclusion chromatography and MALLS. Figure 2a shows a single peak each for $Swa_{MONOMER}$(206−297) and Swa_{DIMER}(206−297) with MALLS-determined molecular masses in good agreement with theoretical molecular masses (14.7 kDa for experimental vs 13.3 kDa for theoretical for a monomer and 27.7 kDa for experimental vs 26.6 kDa for theoretical for a dimer).

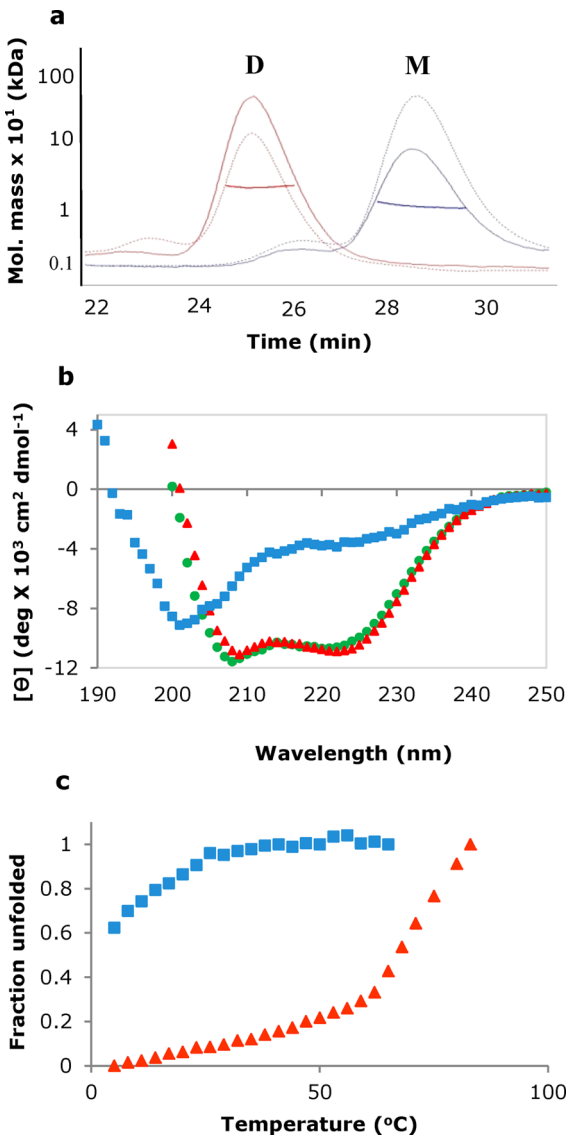

Figure 2. Association state and stability of Swallow constructs. (a) Elution profiles of $Swa_{MONOMER}$(206−297) (M) and Swa_{DIMER}(206−297) (D) shown as overlays of the UV signal at 220 nm and the refractive index. The MALLS analysis is shown as horizontal lines. (b) Far-UV CD profiles of $Swa_{MONOMER}$(206−297) (blue), Swa_{WT} (green), and Swa_{DIMER}(206−297) (red). (c) Thermal unfolding profiles of $Swa_{MONOMER}$(206−297) (blue) and Swa_{DIMER}(206−297) (red) monitored at 222 nm. $Swa_{MONOMER}$(206−297) is predominantly unfolded.

Circular dichroism (CD) differentiates between single and supercoiled helices on the basis of the ratio of ellipticity at 222 and 208 nm. CD spectra of $Swa_{MONOMER}$(206−297), Swa_{DIMER}(206−297), and Swa_{WT} are shown in Figure 2b. While both Swa_{DIMER}(206−297) and Swa_{WT} show double minima at 208 and 222 nm characteristic of an α-helical conformation, Swa_{DIMER}(206−297) has a higher $[\theta_{222}]/[\theta_{208}]$ ratio (close to 1), characteristic of supercoiling and similar to that of the spectra of LC8 bound to Swa_{WT}.[14] $Swa_{MONOMER}$(206−297), in contrast, shows a limited signal at 222 nm and a strong negative peak at 201 nm indicative of a primarily disordered protein. No increase in the level of CD-detected structure was observed in the concentration range of 10−30 μM (spectrum in Figure 2b recorded at 30 μM). At 5 °C, a small increase in the level of helical structure is inferred from an increase in negative ellipticity at 222 nm (Figure 2c) and a small shift in the minima from 201 to 203 nm (data not shown).

The relative stabilities of Swa_{DIMER}(206−297) and $Swa_{MONOMER}$(206−297) were determined from their melting curves at 222 nm (Figure 2c). $Swa_{MONOMER}$(206−297) is fully unfolded above 25 °C, while Swa_{DIMER}(206−297) is considerably more stable and does not detectably unfold below 60 °C. Superimposable melting curves for protein concentrations of 3 and 30 μM indicate a stable dimer at concentrations above 3 μM (data not shown).

Interactions of LC8 with Swallow. Coexpression of LC8 with Swa_{WT} significantly increases the recombinant expression level of soluble Swa_{WT}. The coexpressed LC8−Swa_{WT} complex elutes as a single peak on a gel filtration column (data not shown), consistent with tight binding between LC8 and Swa_{WT}, and has a MALLS-determined molecular mass of 50 kDa, in good agreement with the theoretical mass of 47.8 kDa for a 1:1 complex of dimeric LC8 and dimeric Swallow.

The thermodynamics of binding of LC8 to Swallow constructs were measured by isothermal titration calorimetry (ITC) (Figure 3). Association parameters ($\Delta G°$, $\Delta H°$, and $-T\Delta S°$) are listed in Table 1 and Figure 4. LC8 binds Swa_{WT} with moderate affinity (K_d of 200 nM at 25 °C), significantly tighter than the binding of LC8 to $Swa_{MONOMER}$(206−297) (K_d of 500 nM) but considerably weaker than the binding to Swa_{DIMER}(206−297) (K_d of 70 nM). All interactions are enthalpically driven (Figure 3 and Table 1). Interestingly, the enthalpy change of binding is the same for both $Swa_{MONOMER}$ and Swa_{DIMER} (−12.2 kcal/mol) and is significantly lower than that of Swa_{WT} (−15.2 kcal/mol), which has the highest favorable enthalpy change and highest unfavorable entropy change. Swa_{DIMER}(206−297) binds LC8 with 7-fold binding enhancement relative to the comparable interaction with $Swa_{MONOMER}$(206−297) ($\Delta\Delta G°$ of −1.1 kcal/mol) (Figure 4).

The enthalpies of binding measurements in the 20−35 °C range give heat capacity ΔC_p values of −0.52 kcal mol^{-1} K^{-1} for Swa_{WT} and −0.15 kcal mol^{-1} K^{-1} for both Swa_{DIMER}(206−297) and $Swa_{MONOMER}$(206−297) (Figure 4 and Table 1). Indistinguishably small ΔC_p values for Swa_{DIMER}(206−297) and $Swa_{MONOMER}$(206−297) are likely due to sequestration from the solvent of atoms at the LC8−Swallow interface. The larger ΔC_p of −0.52 for Swa_{WT} reflects additional transfer from solvent or adoption of ordered structure distant from the LC8−Swallow interface.

dx.doi.org/10.1021/bi400642u | *Biochemistry* 2013, 52, 6011−6020

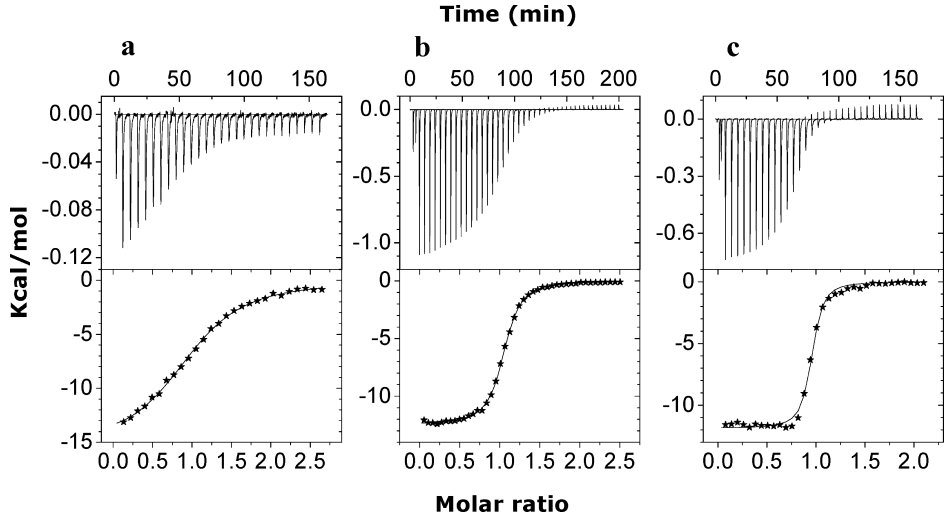

Figure 3. Representative ITC plots for Swallow–LC8 interactions. Thermograms (top) and binding isotherms (bottom) are shown for the titration of (a) Swa_{WT}, (b) $Swa_{MONOMER}(206–297)$, and (c) $Swa_{DIMER}(206–297)$ with LC8. Data were collected at 25 °C and pH 7.4.

Table 1. Thermodynamic Parameters for the Association of Swallow Constructs with LC8 at 25 °C[a]

	K_d (nM)	$\Delta G°$ (kcal/mol)	$\Delta H°$ (kcal/mol)	$-T\Delta S°$ (kcal/mol)	ΔC_p (kcal mol^{-1} K^{-1})
Swa_{WT}	200 ± 20	−9.1 ± 0.9	−15.2 ± 0.1	6.1 ± 1.8	−0.52
$Swa_{MONOMER}$	500 ± 10	−8.6 ± 0.3	−12.3 ± 0.1	3.7 ± 0.2	−0.15
Swa_{DIMER}	70 ± 10	−9.7 ± 0.6	−12.2 ± 0.1	2.5 ± 0.3	−0.15

[a]Average values are reported with errors estimated as the standard deviation from three independent measurements.

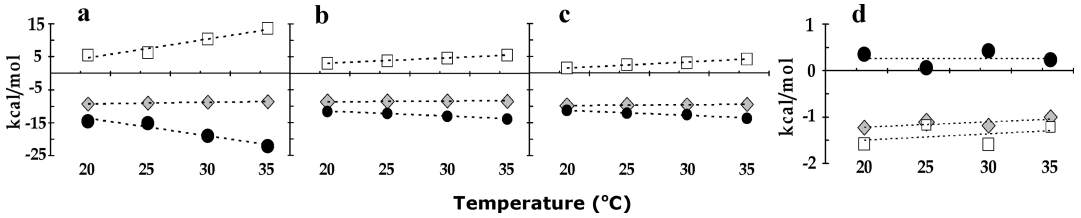

Figure 4. Plots of thermodynamic association parameters [$\Delta G°$ (gray diamonds), $\Delta H°$ (●), and $-T\Delta S°$ (□)] vs temperature for LC8 binding to (a) Swa_{WT}, (b) $Swa_{MONOMER}(206–297)$, and (c) $Swa_{DIMER}(205–297)$. Differences in thermodynamic association parameters [$\Delta\Delta G°$ (gray diamonds), $\Delta\Delta H°$ (●), and $-T\Delta\Delta S°$ (□)] vs temperature between binding of LC8 to $Swa_{MONOMER}$ and Swa_{DIMER} are shown in panel d.

NMR Analysis of $Swa_{DIMER}(205–275)$. The $^{1}H–^{15}N$ HSQC spectrum of $Swa_{DIMER}(205–275)$ with amide backbone resonance assignments of 69 of the expected 71 residues is shown in Figure 5. Secondary structure propensities (SSPs) calculated from Cα and Cβ chemical shifts (Figure 6a) show that residues 216–234 and 249–265 have the highest positive SSP scores indicating the strongest helical propensity. Residues in the middle (235–248) have relatively lower SSP scores that interestingly correspond to residues with weaker coiled-coil prediction (the white segment of the bar at the top of Figure 6). Much lower SSP scores mark both termini indicating disorder at the chain ends.

Backbone dynamics of $Swa_{DIMER}(205–275)$ were determined from ^{15}N R_1 (longitudinal) and R_2 (transverse) relaxation and steady-state heteronuclear NOE spectra. R_1 values, which provide information about the overall molecular motions, are higher at the N- and C-termini and for residues 220, 238, and 243, indicating more flexibility and heterogeneity in these regions relative to the rest of the protein (Figure 6b). R_2 values that are sensitive to internal motions are lower at both the N- and C-termini indicating large-amplitude backbone motions on the subnanosecond time scale, consistent with disordered structure (Figure 6c). Additionally, relatively low R_2 values for some residues and a nonuniform R_2/R_1 ratio within the sequence indicate significant heterogeneity in the middle regions. Negative NOE values at the C-terminus indicate full disorder (Figure 6e).

In dimeric coiled coils, the major contributors to intermonomer NOEs are expected to involve residues at the *a* and *d* positions of the heptad repeats, as these positions are occupied by hydrophobic amino acids packed in a "knob to holes" manner to form a supercoiled α-helix. Approximately 25 intermonomer NOEs were observed in a 3D $\omega1$-$^{13}C/^{15}N$-filtered, ^{13}C-separated NOESY-HSQC spectrum from which 13 were unambiguously assigned. $^{13}C–^{1}H$ intermonomer NOE peak strips are shown for those that are assigned and mapped as a discontinuous stretch to the *a* and *d* positions along the length of the predicted coiled coil (Figure 7).

DISCUSSION

Binding of LC8 Assists Swa_{WT} Folding. The Swa_{WT} construct, expressed primarily in inclusion bodies, has limited solubility (<10 μM) and is primarily monomeric and disordered at physiological temperature.[14] In contrast, Swa_{WT}

dx.doi.org/10.1021/bi400642u | *Biochemistry* 2013, 52, 6011–6020

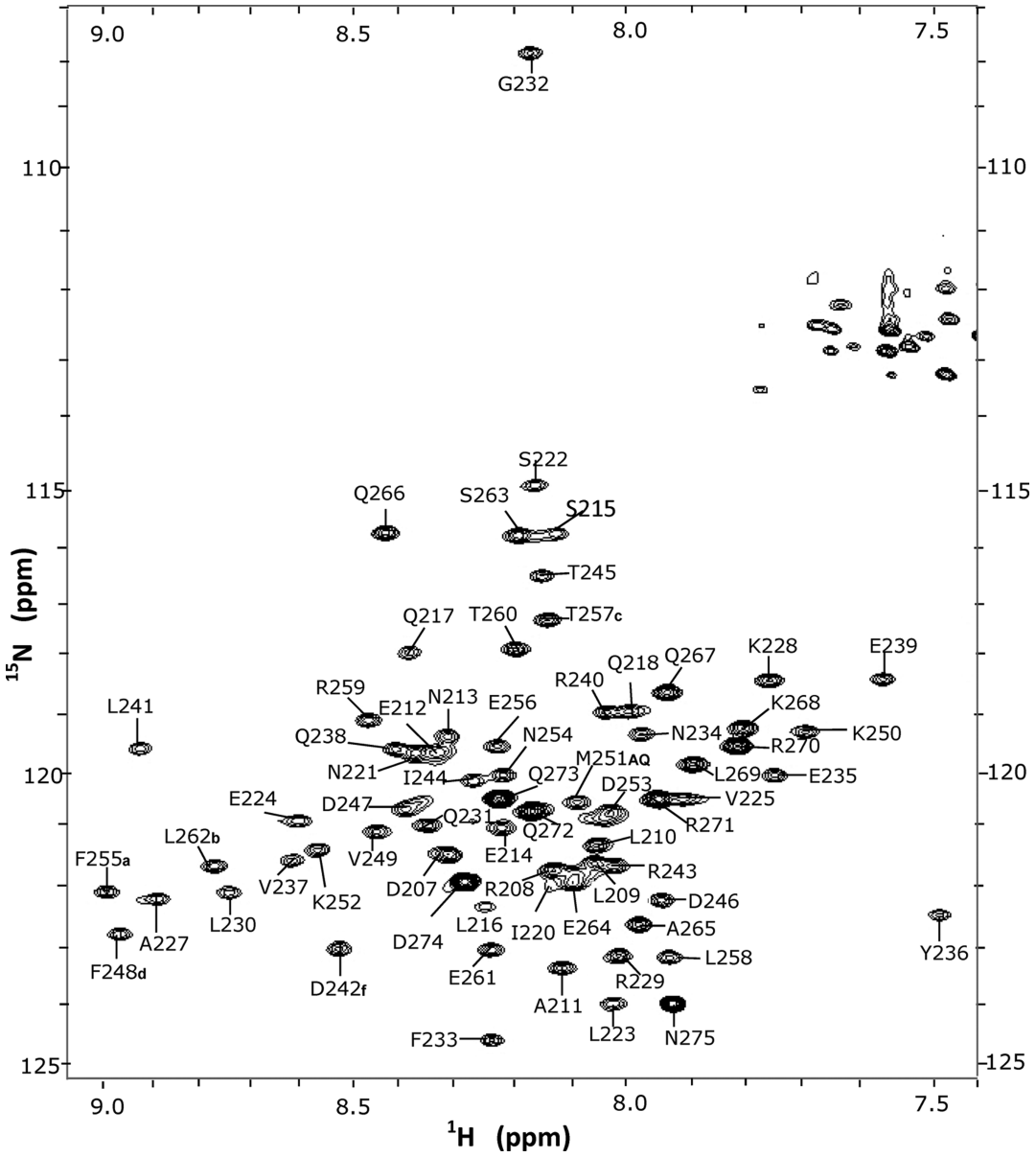

Figure 5. ^{1}H−^{15}N HSQC spectrum of Swa_{DIMER}(205−275) showing assignments. Data were collected at 40 °C on a 950 MHz Bruker Avance III NMR spectrometer.

coexpressed with LC8 is produced in high yield and is soluble even at >500 μM, an indication that LC8 binding aids the folding and solubility of Swa_{WT} during expression in the cell, and *in vitro* after purification. This increase in solubility is not observed when Swa_{WT} is coexpressed with $LC8_{S88E}$, a phosphomimetic mutant of LC8 with weak binding to Swa_{WT}, suggesting that tight binding of LC8 facilitates *in vivo* Swallow folding and protection from aggregation.

The Swallow Self-Association Domain Is a Coiled Coil. Engineered stabilizing mutations based on a hypothetical coiled-coil helical wheel result in a stable dimer, Swa_{DIMER}(206−297), with a melting profile (Figure 2c) suggestive of dissociation coupled to unfolding, characteristic of a stable coiled-coil/leucine zipper dimer.[32] This is in contrast to the two-step melting profile observed for Swa_{WT} that is an equilibrium mixture of monomers and dimers.[14] Engineered destabilizing mutations designed on the basis of a hypothetical coiled-coil helical wheel result in a fully monomeric and primarily unfolded protein. The stability behavior of variants produced with the design assumption of a coiled coil strongly supports the conclusion that in the naturally occurring sequence this domain acquires a coiled-coil configuration that is in register with a wheel based on the predicted coiled coil.

Swa_{DIMER}(205−275) has a thermal stability and dissociation profile similar to LC8-bound Swa_{WT}, and because of the relative ease of its NMR characterization, Swa_{DIMER}(205−275) is used as a model for Swa_{WT} when bound to LC8. The NMR secondary chemical shifts indicate the highest helical propensities for residues 216−234 and 249−265, relatively lower propensities for residues 207−215 and 235−248, and full disorder for the C-terminal segment of residues 270−275. Intermonomer NOEs are consistent with the hypothetical wheel for a dimeric coiled coil. Dynamic measurements indicate disorder at the termini and some heterogeneity in the middle regions. Other evidence in support of a coiled coil is the elongated structure inferred from hydrodynamics measure-

dx.doi.org/10.1021/bi400642u | *Biochemistry* 2013, 52, 6011−6020

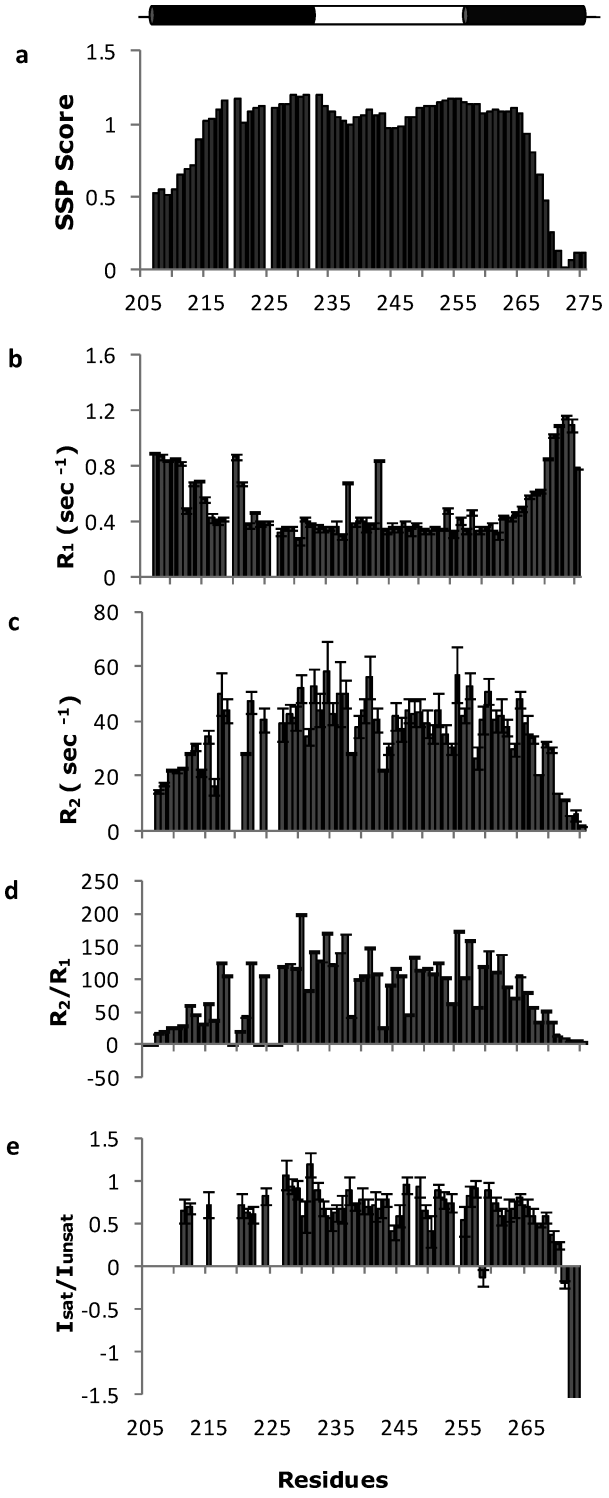

Figure 6. Secondary structure propensities and dynamics of Swa_{DIMER}(205−275). (a) Sequence-based coiled-coil prediction (top bar) shows high coiled-coil propensities for residues 206−232 and 256−275 (black) and relatively lower coiled-coil propensities for residues 233−255 (white). Secondary chemical shift-determined helical propensities are shown in the bar graph as SSP scores per residue. Plots of R_1, R_2, R_2/R_1, and steady-state heteronuclear NOE obtained at 40 °C are shown in panels b−e, respectively. In panel e, the steady-state heteronuclear NOE values below −1.5 for the C-terminal residues are truncated.

ments, and the supercoiling from circular dichroism spectra (Figure 2b). In the absence of a 3D structure, these data provide strong indication of a coiled coil self-association mode for Swallow, with some deviation from standard coiled-coil structure for middle residues.

LC8 Binding Is Coupled to Swallow Self-Association. Thermodynamic coupling of LC8 binding and Swallow self-association is manifested by the significantly larger ΔC_p associated with binding of LC8 to Swa_{WT} (−0.52 kcal mol^{-1} K^{-1}) relative to Swa_{DIMER}(206−297) and $Swa_{MONOMER}$(206−297) (ΔC_p of −0.15 kcal mol^{-1} K^{-1} for both). Heat capacity is a measure of the extent of the burial and dehydration of molecular surfaces from surrounding solvent molecules upon intermolecular association.[33,34] The 0.37 kcal mol^{-1} K^{-1} difference in ΔC_p suggests that for Swa_{WT}−LC8 binding there is additional folding, rigidity, and/or sequestration of atoms from solvent compared to those for binding of LC8 to fully dimeric and fully monomeric Swallow constructs. This is consistent with the expectations that for Swa_{DIMER}(206−297) a coiled coil is already formed and for $Swa_{MONOMER}$(206−297) a coiled coil never forms. The large unfavorable ΔS and large favorable ΔH observed for binding of LC8 to Swa_{WT}, compared to those for binding of LC8 to Swa_{DIMER}(206−297) and $Swa_{MONOMER}$(206−297), are consistent with the interpretation that only in Swa_{WT} are there structural changes in the self-association domain upon LC8 binding. However, a −0.37 kcal mol^{-1} K^{-1} value for self-association of the coiled coil is somewhat lower than expected for a coiled-coil domain of this size. Heat capacity measurements of heterodimerization of leucine zippers, for example, show significantly higher ΔC_p values (−0.7 kcal mol^{-1} K^{-1} for a 30-amino acid peptide to −1.1 kcal mol^{-1} K^{-1} for a 54-amino acid peptide).[32,35] The ΔC_p of unfolding of a homodimeric coiled coil gives a similar value (∼1 kcal mol^{-1} K^{-1} for a 30-amino acid peptide).[32] By this measure, a −0.37 kcal mol^{-1} K^{-1} value would correspond to formation of 16−18 tightly packed amino acids of the 60 predicted amino acids. One explanation for the lower than expected ΔC_p value for the formation of a coiled coil of this size is that a percentage of the Swa_{WT} is already dimeric, and the −0.37 kcal mol^{-1} K^{-1} value is a measure of only ∼70% of the total population. Another is that the monomer is not fully unfolded as in the model coiled-coil proteins studied, and therefore, there is already some sequestration from solvent in the monomer before self-association. A third is that the coiled coil formed is not as tightly packed as the Fos/Jun leucine zipper, for example. Destabilizing interactions such as those observed in Swa_{WT} (between K219 and R224, and because of the positioning of K244 at the hydrophobic interface) could contribute to a lower ΔC_p.[36] The NMR dynamics data confirm a helical coiled coil structure along the length of the predicted coiled coil but also show significant heterogeneity within the coiled coil. Taken together, the most likely interpretation is that the presence of small population of a preexisting dimer and the heterogeneity within the entire coiled coil together contribute to the lower ΔC_p value.

Polybivalency in LC8−Swallow Interactions. Binding enhancement arising from bivalency is implied from the difference in LC8 affinity for Swa_{DIMER}(206−297) versus $Swa_{MONOMER}$(206−297). Both proteins are expected to adopt the same β-strand structure at the LC8−Swa interface but differ in their structure distant from the LC8 binding site. Swa_{DIMER}(206−297), a tightly associated coiled coil, is a bivalent binding partner with two aligned recognition

dx.doi.org/10.1021/bi400642u | Biochemistry 2013, 52, 6011−6020

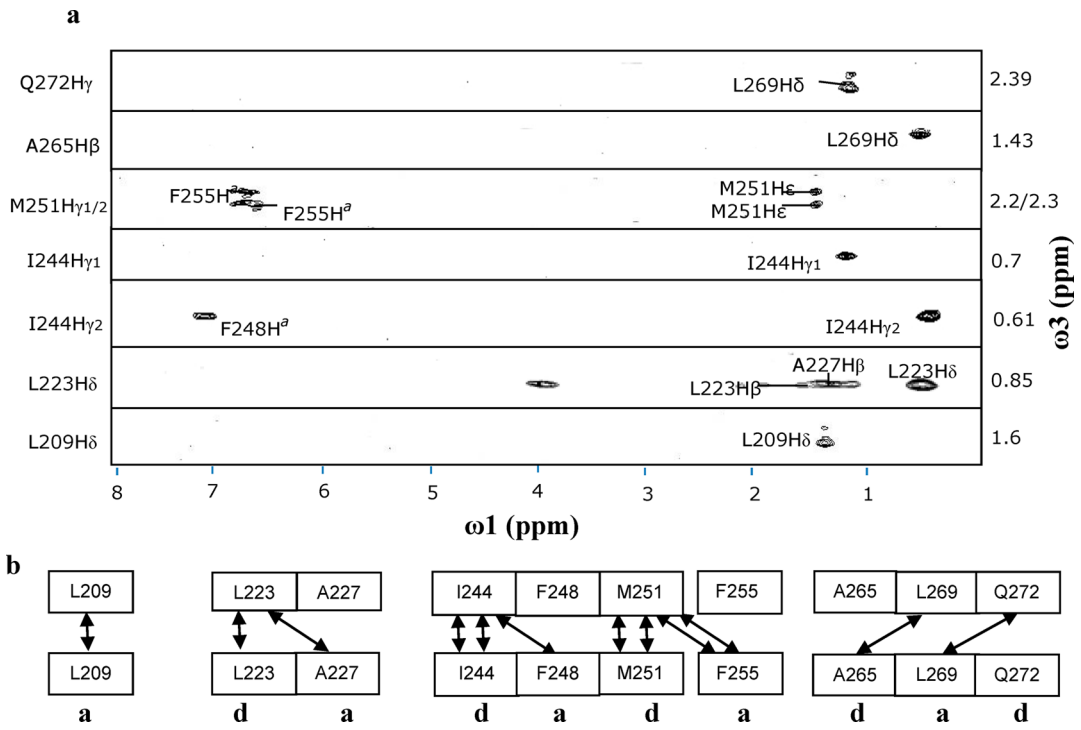

Figure 7. Assignments of intermonomer NOEs. (a) Select $^{1}H-^{13}C$ intermonomer NOE strips from the 3D $\omega1$-$^{13}C/^{15}N$-filtered, ^{13}C-separated NOESY-HSQC spectrum identifying NOEs at the dimer interface of $Swa_{DIMER}(205–275)$. Assignments for aromatic protons are indicated by *a*. (b) NOEs across the hypothetical dimeric coiled-coil interface are shown by arrows and correspond to residues at the *a* and *d* positions. Only the NOEs that are unambiguously assigned are shown in this plot.

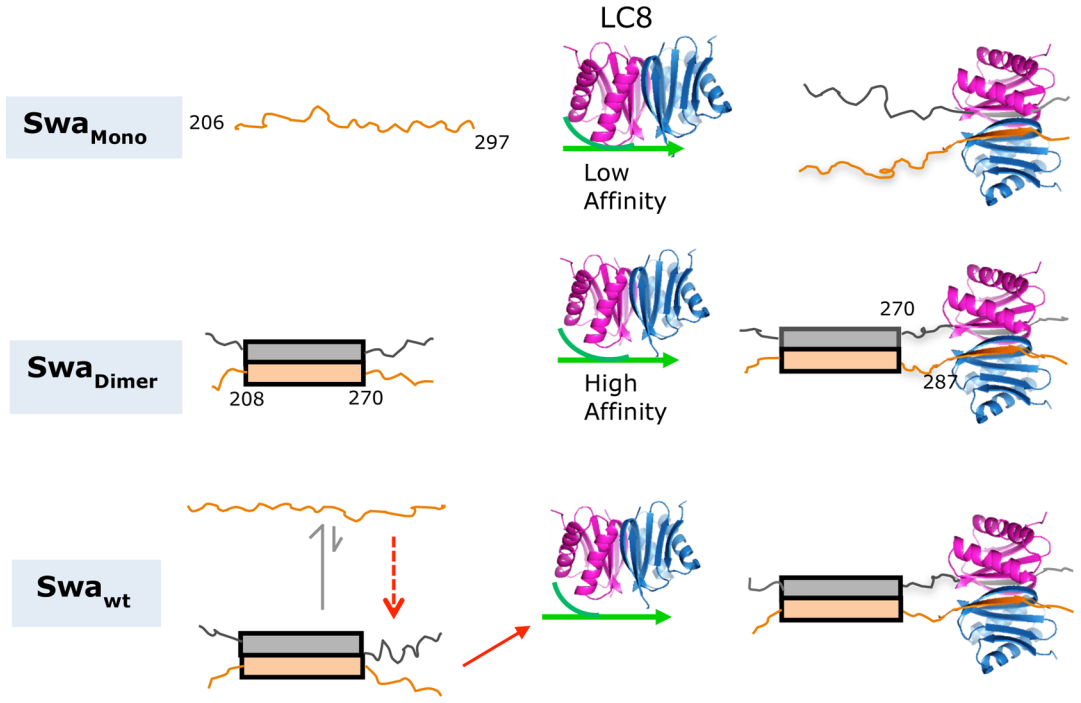

Figure 8. Model showing interactions of LC8 with $Swa_{MONOMER}(206–297)$, $Swa_{DIMER}(206–297)$, and Swa_{WT} and demonstrating that burial from solvent distant from the LC8–Swallow interface occurs only with Swa_{WT}. Bars indicate the helical coiled-coil domain, and lines indicate disorder. Swa_{WT} is a mixture of a high-affinity dimer and a low-affinity monomer. One model that explains how LC8 binding promotes dimer formation is that LC8 binds the small dimeric population and by mass action shifts the population of the bound to fully dimeric. LC8 and LC8–Swa structures are based on Protein Data Bank entries 3BRI and 3E2B[12] and were generated using PyMOL.[43]

sequences for LC8. $Swa_{MONOMER}(206–297)$ is a disordered monovalent chain with one LC8 recognition motif (Figure 8). A 17-residue linker separates the end of the coiled coil [residue 270 (this work)] from the beginning of the LC8 site (residue 287).[8] The binding enhancement of 7-fold is primarily of entropic origin ($\Delta\Delta G°$ of −1.1 kcal/mol, $T\Delta\Delta S°$ of −1.2 kcal/

dx.doi.org/10.1021/bi400642u | *Biochemistry* 2013, 52, 6011–6020

mol, and $\Delta\Delta H$ and $\Delta\Delta C_p$ values of 0) (Figure 4d), as expected from a bivalency effect.[37]

Binding enhancement arising from bivalency appears to be common in the assembly of protein complexes with a high degree of intrinsic disorder. In dynein assembly, binding of the first light chain to a disordered domain of the intermediate chain IC creates a bivalent IC that binds the second light chain with 50-fold enhancement.[38] IC recognition sites for the dimeric light chains LC8 and Tctex1 are separated by a three-residue linker. Also in IC, stabilizing a weak self-association domain C-terminal to the LC8 recognition site results in a 6-fold enhancement of LC8 binding.[22] In the nuclear pore protein Nup159, LC8 binds a disordered domain located between a Phe-Gly repeat and a predicted coiled coil domain to form a structure in which five LC8 homodimers align two extended Nup159 chains.[24] The first binding event is weak, and the bivalency effect is manifested in binding enhancement of successive events.[23] We hypothesize that bivalency effects analogous to those in the binding of LC8 to IC and Nup159 also occur in the case of Swallow. In these examples, bivalency involves not only interactions between intrinsically disordered chains and bivalent protein dimers but also self-association of coiled coil domains. Binding of disordered proteins is associated with a large entropic penalty: the first binding event pays the entropic cost so either the binding affinity of the next ligand is significantly enhanced [e.g., coiled coil formation and LC8 binding (this work)] or the first binding may compensate for unfavorable interactions caused by repulsive interactions (e.g., the IC−Tctex1 interface[38]) or for increased protein rigidity (e.g., Nup159−LC8 assembly[23]).

Functional Implications. What are the implications of LC8-promoted coiled-coil formation in Swallow function? Genetic experiments with *Drosophila* ovaries show that the distribution of *bcd* mRNA during oogenesis and early embryogenesis depends on the interaction of LC8 with Swallow. A Swallow mutant lacking the coiled coil domain and the LC8 recognition motif shows no localization of *bcd* mRNA.[1] Interestingly, naturally occurring *swa* alleles with mutations in the protein's C-terminal domain also show defects in *bcd* mRNA localization. These mutations abolish correct Swallow localization but not LC8 binding, suggesting that the primarily disordered C-terminal domain plays a critical role in localization. Coiled-coil-mediated protein interactions are involved in a variety of biological processes, including vesicle-mediated transport, cellular membrane organization, cytokinesis, and chromosome segregation.[39] Dimerization by formation of a coiled coil either increases the avidity for binding partners as in SCAB1[40] or allosterically promotes formation of a structured domain conducive for binding, such as inducing formation of a voltage-gated channel assembly.[41] With Swallow, the LC8-promoted coiled coil suggests an intriguing potential for further bivalency effects that could allosterically induce structural organization of the disordered N- and C-terminal domains and thus underlie the essential role of LC8−Swallow interactions in bicoid localization.

AUTHOR INFORMATION

Corresponding Author

*Department of Biochemistry and Biophysics, Oregon State University, Corvallis, OR 97331. E-mail: barbare@science.oregonstate.edu. Telephone: (541) 737-4143. Fax: (541) 737-0481.

Present Address

§J.H.: Pfizer Global Research and Development, Eastern Point Road, Groton, CT 06340.

Funding

This work is supported by National Institutes of Health Grant GM 084276.

Notes

The authors declare no competing financial interest.

ACKNOWLEDGMENTS

We acknowledge the support of the nucleic acid and protein core and the mass spectrometry facilities and services core in the Oregon State University Environmental Health Sciences Center (National Institute of Environmental Health Sciences Grant 00210), Adrien Favier at the Institut de Biologie Structurale and the TGIR-RMN-THC Fr3050 CNRS (Grenoble, France), and access to the Research Infrastructure activity in the 7th Framework Programme of the EC (Project 261863, Bio-NMR) (Frankfurt, Germany).

ABBREVIATIONS

Swa, Swallow; *bcd* mRNA, bicoid mRNA; Swa_{WT}, wild-type Swallow construct corresponding to amino acids 206−297; LC8, dynein light chain; IC, dynein intermediate chain; Nup159, nucleoporin 159; ITC, isothermal titration calorimetry; CD, circular dichroism; MALLS, multiangle laser light scattering; HSQC, heteronuclear single-quantum coherence; TOCSY, total correlation spectroscopy; NOE, nuclear Overhauser effect; ΔC_p, change in heat capacity.

REFERENCES

(1) Schnorrer, F., Bohmann, K., and Nusslein-Volhard, C. (2000) The molecular motor dynein is involved in targeting swallow and bicoid RNA to the anterior pole of *Drosophila* oocytes. *Nat. Cell Biol. 2*, 185−190.

(2) Schnorrer, F., Luschnig, S., Koch, I., and Nusslein-Volhard, C. (2002) γ-Tubulin37C and γ-tubulin ring complex protein 75 are essential for bicoid RNA localization during drosophila oogenesis. *Dev. Cell 3*, 685−696.

(3) Hays, T., and Karess, R. (2000) Swallowing dynein: A missing link in RNA localization? *Nat. Cell Biol. 2*, E60−E62.

(4) Meng, J., and Stephenson, E. C. (2002) Oocyte and embryonic cytoskeletal defects caused by mutations in the *Drosophila* swallow gene. *Dev. Genes Evol. 212*, 239−247.

(5) Pokrywka, N. J., Fishbein, L., and Frederick, J. (2000) New phenotypes associated with the swallow gene of *Drosophila*: Evidence for a general role in oocyte cytoskeletal organization. *Dev. Genes Evol. 210*, 426−435.

(6) Berleth, T., Burri, M., Thoma, G., Bopp, D., Richstein, S., Frigerio, G., Noll, M., and Nusslein-Volhard, C. (1988) The role of localization of bicoid RNA in organizing the anterior pattern of the *Drosophila* embryo. *EMBO J. 7*, 1749−1756.

(7) Driever, W., and Nusslein-Volhard, C. (1988) A gradient of bicoid protein in *Drosophila* embryos. *Cell 54*, 83−93.

(8) Benison, G., Karplus, P. A., and Barbar, E. (2007) Structure and dynamics of LC8 complexes with KXTQT-motif peptides: Swallow and dynein intermediate chain compete for a common site. *J. Mol. Biol. 371*, 457−468.

(9) Benison, G., Nyarko, A., and Barbar, E. (2006) Heteronuclear NMR identifies a nascent helix in intrinsically disordered dynein intermediate chain: Implications for folding and dimerization. *J. Mol. Biol. 362*, 1082−1093.

(10) Makokha, M., Hare, M., Li, M., Hays, T., and Barbar, E. (2002) Interactions of cytoplasmic dynein light chains Tctex-1 and LC8 with the intermediate chain IC74. *Biochemistry 41*, 4302−4311.

(11) Harrison, A., and King, S. M. (2000) The molecular anatomy of dynein. *Essays Biochem. 35*, 75−87.
(12) Benison, G., Karplus, P. A., and Barbar, E. (2008) The interplay of ligand binding and quaternary structure in the diverse interactions of dynein light chain LC8. *J. Mol. Biol. 384*, 954−966.
(13) Williams, J. C., Roulhac, P. L., Roy, A. G., Vallee, R. B., Fitzgerald, M. C., and Hendrickson, W. A. (2007) Structural and thermodynamic characterization of a cytoplasmic dynein light chain-intermediate chain complex. *Proc. Natl. Acad. Sci. U.S.A. 104*, 10028−10033.
(14) Wang, L., Hare, M., Hays, T. S., and Barbar, E. (2004) Dynein light chain LC8 promotes assembly of the coiled-coil domain of swallow protein. *Biochemistry 43*, 4611−4620.
(15) Lo, K. W., Kan, H. M., Chan, L. N., Xu, W. G., Wang, K. P., Wu, Z., Sheng, M., and Zhang, M. (2005) The 8-kDa dynein light chain binds to p53-binding protein 1 and mediates DNA damage-induced p53 nuclear accumulation. *J. Biol. Chem. 280*, 8172−8179.
(16) Barbar, E. (2008) Dynein light chain LC8 is a dimerization hub essential in diverse protein networks. *Biochemistry 47*, 503−508.
(17) Weil, T. T., Xanthakis, D., Parton, R., Dobbie, I., Rabouille, C., Gavis, E. R., and Davis, I. (2010) Distinguishing direct from indirect roles for bicoid mRNA localization factors. *Development 137*, 169−176.
(18) Stephenson, E. C. (2004) Localization of swallow-Green Fluorescent Protein in *Drosophila* oogenesis and implications for the role of swallow in RNA localization. *Genesis 39*, 280−287.
(19) Schmidt, J. C., Kiyomitsu, T., Hori, T., Backer, C. B., Fukagawa, T., and Cheeseman, I. M. (2010) Aurora B kinase controls the targeting of the Astrin-SKAP complex to bioriented kinetochores. *J. Cell Biol. 191*, 269−280.
(20) Vadlamudi, R. K., Bagheri-Yarmand, R., Yang, Z., Balasenthil, S., Nguyen, D., Sahin, A. A., den Hollander, P., and Kumar, R. (2004) Dynein light chain 1, a p21-activated kinase 1-interacting substrate, promotes cancerous phenotypes. *Cancer Cell 5*, 575−585.
(21) Rayala, S. K., den Hollander, P., Manavathi, B., Talukder, A. H., Song, C., Peng, S., Barnekow, A., Kremerskothen, J., and Kumar, R. (2006) Essential role of KIBRA in co-activator function of dynein light chain 1 in mammalian cells. *J. Biol. Chem. 281*, 19092−19099.
(22) Nyarko, A., and Barbar, E. (2011) Light chain-dependent self-association of dynein intermediate chain. *J. Biol. Chem. 286*, 1556−1566.
(23) Nyarko, A., Song, Y., Novacek, J., Zidek, L., and Barbar, E. (2013) Multiple recognition motifs in nucleoporin Nup159 provide a stable and rigid Nup159-Dyn2 assembly. *J. Biol. Chem. 288*, 2614−2622.
(24) Stelter, P., Kunze, R., Flemming, D., Hopfner, D., Diepholz, M., Philippsen, P., Bottcher, B., and Hurt, E. (2007) Molecular basis for the functional interaction of dynein light chain with the nuclear-pore complex. *Nat. Cell Biol. 9*, 788−796.
(25) Song, Y., Benison, G., Nyarko, A., Hays, T. S., and Barbar, E. (2007) Potential role for phosphorylation in differential regulation of the assembly of dynein light chains. *J. Biol. Chem. 282*, 17272−17279.
(26) Lescop, E., Kern, T., and Brutscher, B. (2010) Guidelines for the use of band-selective radiofrequency pulses in hetero-nuclear NMR: Example of longitudinal-relaxation-enhanced BEST-type ^{1}H-^{15}N correlation experiments. *J. Magn. Reson. 203*, 190−198.
(27) Goddard, T. D., and Kneller, D. G. *SPARKY3*, University of California, San Francisco.
(28) Johnson, B. A. (2004) Using NMRView to visualize and analyze the NMR spectra of macromolecules. *Methods Mol. Biol. 278*, 313−352.
(29) Marsh, J. A., Singh, V. K., Jia, Z., and Forman-Kay, J. D. (2006) Sensitivity of secondary structure propensities to sequence differences between α- and γ-synuclein: Implications for fibrillation. *Protein Sci. 15*, 2795−2804.
(30) Lupas, A., Van Dyke, M., and Stock, J. (1991) Predicting coiled coils from protein sequences. *Science 252*, 1162−1164.
(31) Breeze, A. L. (2000) Isotope-filtered NMR methods for the study of biomolecular structure and interactions. *Prog. Nucl. Magn. Reson. Spectrosc. 36*, 323−372.
(32) Jelesarov, I., and Bosshard, H. R. (1996) Thermodynamic characterization of the coupled folding and association of heterodimeric coiled coils (leucine zippers). *J. Mol. Biol. 263*, 344−358.
(33) Murphy, K. P., and Freire, E. (1992) Thermodynamics of structural stability and cooperative folding behavior in proteins. *Adv. Protein Chem. 43*, 313−361.
(34) Spolar, R. S., and Record, M. T., Jr. (1994) Coupling of local folding to site-specific binding of proteins to DNA. *Science 263*, 777−784.
(35) Seldeen, K. L., McDonald, C. B., Deegan, B. J., and Farooq, A. (2008) Thermodynamic analysis of the heterodimerization of leucine zippers of Jun and Fos transcription factors. *Biochem. Biophys. Res. Commun. 375*, 634−638.
(36) Steif, C., Hinz, H. J., and Cesareni, G. (1995) Effects of cavity-creating mutations on conformational stability and structure of the dimeric 4-α-helical protein ROP: Thermal unfolding studies. *Proteins 23*, 83−96.
(37) Jencks, W. P. (1981) On the attribution and additivity of binding energies. *Proc. Natl. Acad. Sci. U.S.A. 78*, 4046−4050.
(38) Hall, J., Karplus, P. A., and Barbar, E. (2009) Multivalency in the assembly of intrinsically disordered dynein intermediate chain. *J. Biol. Chem. 284*, 33115−33121.
(39) Wang, Y., Zhang, X., Zhang, H., Lu, Y., Huang, H., Dong, X., Chen, J., Dong, J., Yang, X., Hang, H., and Jiang, T. (2012) Coiled-coil networking shapes cell molecular machinery. *Mol. Biol. Cell 23*, 3911−3922.
(40) Zhang, W., Zhao, Y., Guo, Y., and Ye, K. (2012) Plant actin-binding protein SCAB1 is dimeric actin cross-linker with atypical pleckstrin homology domain. *J. Biol. Chem. 287*, 11981−11990.
(41) Fujiwara, Y., Kurokawa, T., Takeshita, K., Kobayashi, M., Okochi, Y., Nakagawa, A., and Okamura, Y. (2012) The cytoplasmic coiled-coil mediates cooperative gating temperature sensitivity in the voltage-gated H^{+} channel Hv1. *Nat. Commun. 3*, 816.
(42) Jones, D. T. (1999) Protein secondary structure prediction based on position-specific scoring matrices. *J. Mol. Biol. 292*, 195−202.
(43) DeLano, W. L. (2002) *The PyMOL Molecular Graphics System*, DeLano Scientific LLC, San Carlos, CA.